

SENSITIVITY ANALYSIS IN AN IMMUNO-EPIDEMIOLOGICAL VECTOR-HOST MODEL

HAYRIYE GULBUDAK[†], ZHUOLIN QU, FABIO MILNER, AND NECIBE TUNCER

ABSTRACT. Sensitivity Analysis (SA) is a useful tool to measure the impact of changes in model parameters on the infection dynamics, particularly to quantify the expected efficacy of disease control strategies. SA has only been applied to epidemic models at the population level, ignoring the effect of within-host virus-with-immune-system interactions on the disease spread. Connecting the scales from individual to population can help inform drug and vaccine development. Thus the value of understanding the impact of *immunological* parameters on epidemiological quantities. Here we consider an age-since-infection structured vector-host model, in which epidemiological parameters are formulated as functions of within-host virus and antibody densities, governed by an ODE system. We then use SA for these immuno-epidemiological models to investigate the impact of immunological parameters on population-level disease dynamics such as *basic reproduction number, final size of the epidemic or the infectiousness at different phases of an outbreak*. As a case study, we consider Rift Valley Fever Disease (RVFD) utilizing parameter estimations from prior studies. SA indicates that 1% increase in within-host pathogen growth rate can lead up to 8% increase in \mathcal{R}_0 , up to 1% increase in steady-state infected host abundance, and up to 4% increase in infectiousness of hosts when the reproduction number \mathcal{R}_0 is larger than one. These significant increases in population-scale disease quantities suggest that control strategies that reduce the within-host pathogen growth can be important in reducing disease prevalence.

KEYWORDS: immuno-epidemiological model, sensitivity analysis, Rift Valley Fever, basic reproduction number, multi-scale model

AMS SUBJECT CLASSIFICATION: 92D30, 92D40

1. INTRODUCTION

Sensitivity Analysis (SA) is a common methodological approach for determining the expected impact of control strategies on common disease outbreak quantities such as final size and basic reproduction number [20]. SA has been used extensively for ODE models but has not been extended to age-structured models. In this study, we develop a method that extends SA to immuno-epidemiological models [23, 13, 10, 2]. We couple a time-since-infection-structured epidemiological system with an ODE immunological model. The main motivation for this modeling approach is that many recent vector-borne epidemic models share the limitation of exploring only between-host transmission while ignoring the impact of within-host virus-with-immune-response interactions, which may be important to guide drug and vaccine development, for example. Here we demonstrate the approach through a multi-scale model, first introduced in [14]. The parameters for this model are studied in [23] based on Rift Valley Fever Disease (RVFD) immunological

Date: November 23, 2021.

[†]author for correspondence.

data and human epidemiological data from the 2006 – 2007 Kenya Outbreak [6, 21]. Using the SA approach developed here, we quantify the impact of within-host parameters on the Rift Valley Fever Disease (RVFD) dynamics. The same multi-scale modeling framework can be adapted to other arbovirus diseases such as Dengue and West Nile Virus (WNV).

RVFD is a viral disease transmitted by mosquitoes, mainly from the *Aedes* and *Culex* genera, and causes illness and death in several different mammal species, including livestock (e.g. cattle, buffalo, sheep, goat, and camel), as well as in humans. RVFD has resulted in significant negative socio-economic impacts, for example, due to abortion among RVF-infected livestock and high mortality among younger ones. In 2018, a panel of experts convened by the World Health Organization (WHO) listed RVF among diseases that pose big public-health risks, yet few or no intervention strategies have been developed. SA can provide helpful insights on the impact of possible pharmaceutical interventions for RVFD control.

Sensitivity analysis has been utilized in several ODE models to assess the impact of epidemic parameters on epidemic quantities. For example, Gaff et al. [9, 8] considered an ODE vector-host RVF model to assess the effectiveness of some control interventions on RVFD. Fischer et al. [5] utilized SA to investigate the effect of temperate climate on the RVFD dynamics. Mpeshe et al. [20] formulated an ODE model of RVF incorporating parameters dependent of human behavior to investigate disease dynamics and explore sensitivity of the model to variation in those parameters. Xiao et al. [24] recently studied the effect of both seasonality and socioeconomic status in a multi-patch model. To the best of our knowledge, the SA of immuno-epidemiological models has never been carried out, despite the value and usefulness of SA of the underlying immunological model parameters on epidemic variables related quantities related to them.

In this study, we develop a novel approach for SA in immuno-epidemiological models to investigate the impact of immunological parameters on the disease dynamics. In particular, we consider a time-since-infection-structured vector-host model in which epidemiological model parameters are described as functions of within-host virus-antibody densities that are governed by an ODE system. We first define the basic reproduction number, \mathcal{R}_0 that serves as a threshold between extinction and persistence of RVFD. Then we use this SA approach to investigate the impact of changes in immunological parameters on epidemic quantities such as basic reproduction number, and final disease abundance when $\mathcal{R}_0 > 1$. Interestingly, our analytical and numerical results suggest that immunological parameters such as viral growth rate and immune activation rate can have a large impact on disease outcomes, underscoring the importance of pharmacological intervention strategies.

This paper is organized as follows. In Section 2, we present an immuno-epidemiological model, first introduced in [14, 23], and summarize the stability and persistence conditions for the disease. In Section 3, we develop a novel approach for SA in immuno-epidemiological models to assess the impact of the within-host parameters on epidemic quantities. Furthermore in subsection 3.2, we consider three distinct stages of an outbreak —initial, peak and die-out— and show how infectiousness of hosts at these different stages of infection is altered by slight changes in the immunological parameters through the phases of an outbreak. In the last section, we summarize our results and draw some conclusions.

2. AN IMMUNO-EPIDEMIOLOGICAL VECTOR-BORNE DISEASE MODEL

A simple model that captures vector-borne disease spread on two-scales (namely immunological and the epidemiological) was first introduced in [14]. At the individual scale, we consider the following immune response model with three state variables representing serum density of the pathogen and of two specific antibodies released by B-cell lymphocytes —IgM and IgG— with densities given, respectively, by $P = P(\tau)$, $M = M(\tau)$ and $G = G(\tau)$, where τ is the time elapsed since infection:

$$(2.1) \quad \frac{dP}{d\tau} = (f(P) - \theta M - \delta G) P, \quad \frac{dM}{d\tau} = (aP - (q + c)) M, \quad \frac{dG}{d\tau} = qM + bGP.$$

The initial values are $P(0) = P_0 > 0$, $M(0) = M_0 \geq 0$, $G(0) = G_0 \geq 0$, and $M_0 + G_0 > 0$ to ensure that there is a pathogen and an immune response. It is assumed that the pathogen replicates with a logistic per capita growth rate $f(P) = r(1 - \frac{P}{K})$ and that, upon exposure to the virus, the IgM and IgG antibodies get activated at unit rates a and b , respectively. The IgM antibodies are responsible for a *quick immunological response (innate)*: they kill virus at a unit rate θ and decay at a unit rate c . The IgG antibodies kill the pathogen at a unit rate δ , and they are mainly responsible for *long-term immunity (adaptive)* [14, 23]. Mature B-cells activated by antigen stimulation proliferate quickly in lymphoid follicles and undergo genetic alterations resulting in a switch of the immunoglobulin isotype produced from IgM to either IgG, IgE, or IgA. To keep the immune response model lower-dimensional, we model the B-cell population indirectly through the IgM and IgG antibodies it produces. We incorporate this switch in antibody production by the B-cells by “converting” IgM antibodies to IgG antibodies at a unit rate q [16]. All parameters and state variables of this within-host model and their definitions are given in Table 2.1 and Table 2.2. Different dynamics of this immune response model can be found in Figure 2.1.

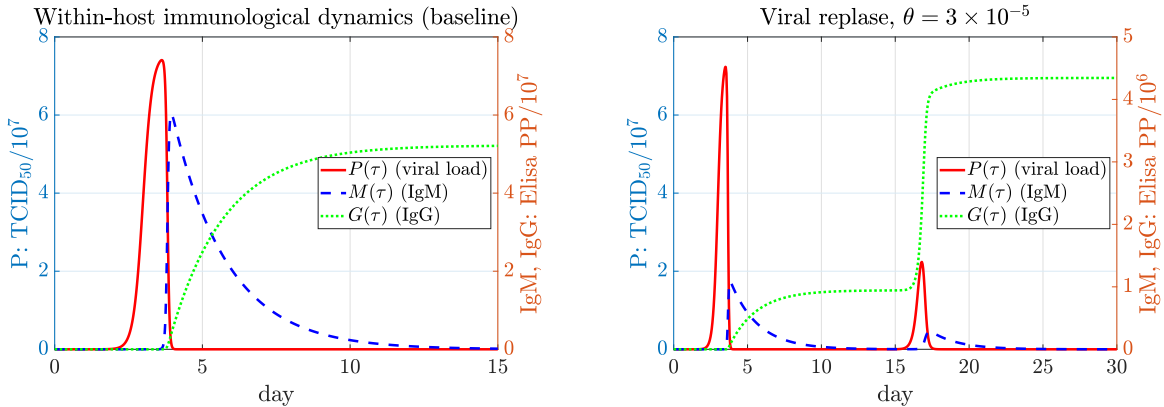


FIGURE 2.1. *Different within-host pathogen-immune response antibody dynamics* **Left.** General within-host dynamics. **Right.** *Resurgence of virus.* The experiments done on monkeys suggest that in some cases, viral load appears to be controlled after an initial infection but makes a resurgence after disseminating into new tissue [22].

A detailed analysis of the immunological model extended to include vector-to-host inoculum size dependent on age-of-infection of vectors was presented in [12]. In general

upon viral progression within an infected mosquito midgut, the amount of pathogen in an infected mosquito's saliva dynamically changes with respect to its infection-age, determining the vector-to-host inoculum size P_0 that is the amount of pathogen injected to a susceptible host by an infectious vector during the infectious contact. Assuming that P_0 is constant, all analytical results therein also hold for our present immunological model. In particular, the following result is established [12]:

Theorem 1. *If $M_0 > 0$ (or $G_0 > 0$), then the pathogen eventually clears ($\lim_{\tau \rightarrow \infty} P(\tau) = 0$), the IgM antibodies decay to zero after viral clearance and, subsequently, the IgG memory antibodies reach a steady-state; i.e. $\lim_{\tau \rightarrow \infty} M(\tau) = 0$ and $\lim_{\tau \rightarrow \infty} G(\tau) = G^+$, where $G^+ > 0$ depends on the initial condition (P_0, M_0, G_0) .*

The innate and adaptive immune responses vary from organism to organism and depend on several factors, including the initial viral dose, the strain of the virus, the age of the host, and the species of the host. However, infections like RVFV in the laboratory generally follow three qualitative scenarios:

- The viral load within the host grows rapidly to high levels within the host, and the host dies.
- There is a delayed onset of complications of infections: e.g. viral load appears to be controlled after an initial infection but makes a resurgence after disseminating into new tissue, such as the central nervous system. This often leads to long-term consequences such as blindness and may also be lethal.
- The viral load within the host is brought under control and annihilated by a robust immune response.

Our immunological model captures the general dynamics of these different infection and immune-response scenarios as seen in Figure 2.1 and as suggested by the analytical result above (Theorem 1). In general, within-host dynamics in arbovirus diseases behave as depicted in Figure 2.1 (left), corresponding to the third scenario mentioned above. Also, in a lab experiment with monkeys infected with RVFV, it was observed that monkeys died when the viral concentration rebounded as seen in Figure 2.1(right). In surviving monkeys, the within-host dynamics imitated the third scenario [19]. In an ideal immune response, the immune system releases virus-specific antibodies, targeting the virus and bringing it to extinction. These dynamics are captured in Figure 2.1 (left). However, sometimes there is a resurgence of virus within the host as the virus spreads into new organs and tissues, such as the central nervous system. This is often associated with delayed onset of symptoms, including blindness, and may result in fatalities [22]. Our model can capture these dynamics as well, as can be seen in Figure 2.1 (right).

At the *population scale*, we consider a time-since-infection structured vector-host model, (2.2), where $S_H(t)$ and $R_H(t)$ are the numbers of susceptible and recovered individuals in the host population and $i_H(\tau, t)$ is the infected-host density, structured by age-of-infection τ . The total number of infected individuals is $I_H(t) = \int_0^\infty i_H(\tau, t) d\tau$. The vector compartments $S_V(t)$ and $I_V(t)$ represent, respectively, the size of susceptible and infected vector populations at time t . The full model is as follows:

$$(2.2) \quad \left\{ \begin{array}{l} \frac{dS_H}{dt} = \Lambda - \beta_V S_H(t) I_V(t) - dS_H(t), \\ \frac{\partial i_H}{\partial t} + \frac{\partial i_H}{\partial \tau} = -(\alpha(\tau) + \kappa(\tau) + \gamma(\tau) + d) i_H(\tau, t), \quad i_H(0, t) = \beta_V S_H(t) I_V(t), \\ \frac{dR_H}{dt} = \int_0^\infty \gamma(\tau) i_H(\tau, t) d\tau - dR_H(t), \\ \frac{dS_V}{dt} = \eta - \left(\int_0^\infty \beta_H(\tau) i_H(\tau, t) d\tau + \mu \right) S_V(t), \\ \frac{dI_V}{dt} = S_V(t) \int_0^\infty \beta_H(\tau) i_H(\tau, t) d\tau - \mu I_V(t). \end{array} \right.$$

To *bridge the scales* from individual to population, the unit infectiousness and the disease-induced death and recovery rates are formulated as functions of immunological variables as suggested by *data* in [15, 7], as follows:

$$(2.3) \quad \left\{ \begin{array}{l} \beta_H(\tau) = \frac{C_\beta P(\tau)}{C_0 + P(\tau)}, \\ \alpha(\tau) = \zeta P(\tau), \\ \kappa(\tau) = \xi M(\tau), \\ \gamma(\tau) = C_\gamma \frac{G(\tau)}{P(\tau) + \epsilon_0}. \end{array} \right.$$

Fig. A.1 in the Appendix shows how some of the corresponding epidemiological parameters evolve over the course of host infection. Note that Tuncer et al.[23] considers mass action term, satisfying *balance equation* for describing the interactions between vectors and hosts with following underlying assumptions:

- $c_v N_v$ = total number of contacts (bites received) per host. Then total number of contacts (bites received) that hosts' have: $(c_v N_v) \times (N_H)$.
- $c_H N_H$ = total number of contacts (given bites) per vector. Then total number of contacts (given bites) that vectors' have: $(c_H N_H) \times (N_v)$. Therefore it makes sense when the host population size is small (or not changing much).
- To satisfy balance equation (conservation law), we assume that $c_v = c_H$.
- Here c is proportionality constant. Mass action assumes that per vector (or per host) contact is proportional to total host (or total vector) population. Therefore it has different meaning than the one in standard incidence.

Changes to the functional form of the interaction terms such as considering *frequency depending force of infection rate* (standard incidence) will be further explored in later work.

A schematic diagram for the full system is presented next in Fig. 2.2.

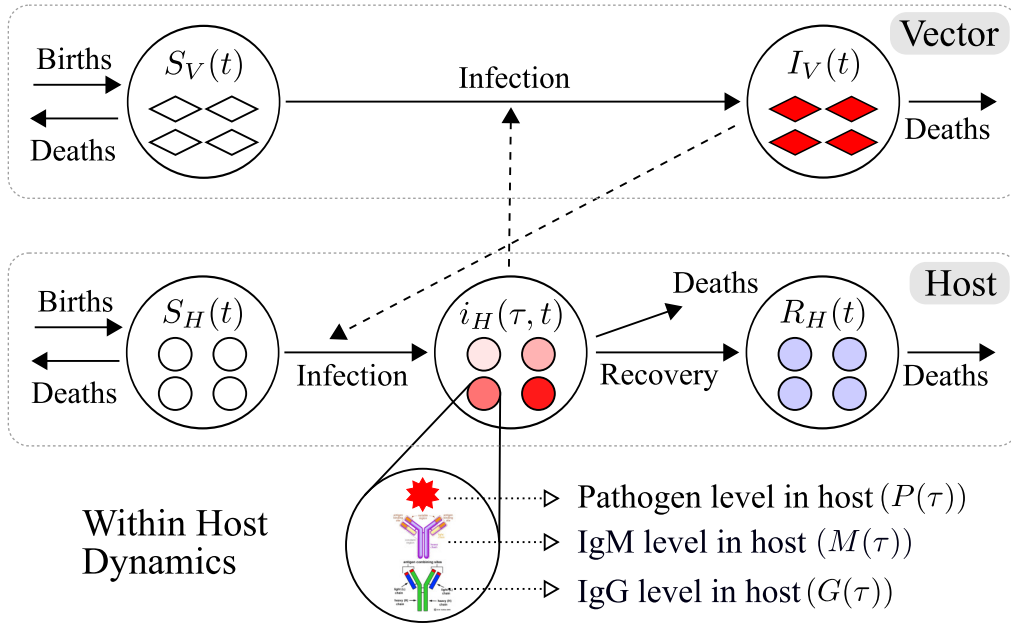


FIGURE 2.2. Schematic illustration of the immuno-epidemiological vector-host model(2.1)-(2.3).

TABLE 2.1. Model parameters: Parameter estimates of the immuno-epidemiological model (2.1)-(2.3) fitted [23]. θ and δ are the killing efficiency parameters that re-scale the population immune cells. * q value is chosen differently (fit separately)

immunological parameters (within-host model (2.1))		dimension	baseline	range
r	Unit pathogen growth rate	day ⁻¹	6.3033	1 ~ 10
K	Carrying capacity of pathogens	TCID ₅₀	7.57×10^7	$1.5 \times 10^7 \sim 10^8$
a	Unit IgM-activation rate per pathogen	(TCID ₅₀ × day) ⁻¹	3.93×10^{-7}	$10^{-8} \sim 5 \times 10^{-7}$
b	Unit IgG-activation rate per pathogen	(TCID ₅₀ × day) ⁻¹	9.58×10^{-8}	$5 \times 10^{-9} \sim 10^{-6}$
θ	Unit IgM pathogen-destruction rate per-pathogen	(Elisa PP × day) ⁻¹	5×10^{-7}	$10^{-9} \sim 10^{-4}$
δ	Unit IgG pathogen-destruction rate per pathogen	(Elisa PP × day) ⁻¹	8.3918×10^{-8}	$1.7 \times 10^{-10} \sim 1.7 \times 10^{-5}$
q	Unit IgM-to-IgG production switch rate	day ⁻¹	0.4232*	2 ~ 20
c	Unit IgM decay rate	day ⁻¹	0.1155	0.01 ~ 1
epidemic parameters (vector-host model (2.2))				
$\Lambda = d$	Host recruitment rate	host × day ⁻¹	1/(365 × 10)	
$\eta = \mu$	Vector recruitment rate	vector × day ⁻¹	1/40	
β_V	Per-capita-per-infected vector transmission rate	(vector × day) ⁻¹	0.2	
$\beta_H(\tau)$	Unit age-of-infection-dependent per host transmission rate	(host × day) ⁻¹	-	
$\alpha(\tau)$	Unit pathogen-induced death rate	day ⁻¹	-	
$\kappa(\tau)$	Unit immune-response-induced death rate	day ⁻¹	-	
$\gamma(\tau)$	Unit recovery rate τ days post-infection	day ⁻¹	-	
d	Unit natural death rate of hosts	day ⁻¹	1/(365 × 10)	
μ	Unit natural death rate of vectors	day ⁻¹	1/40	
linking function parameters (2.3)				
C_β	transmission efficiency of pathogen infection	(host × day) ⁻¹	0.5365	
C_0	half-saturation constant in transmission rate	TCID ₅₀	3.03×10^3	
ζ	unit per host pathogen-lethality rate	(TCID ₅₀ × day) ⁻¹	6.21×10^{-8}	
ξ	unit per host immune-response-lethality rate	(Elisa PP × day) ⁻¹	8.51×10^{-5}	
C_γ	recovery coefficient	$\frac{\text{TCID}_{50}}{\text{Elisa PP} \times \text{day}}$	0.7212	
ϵ_0	half-saturation constant in recovery rate	TCID ₅₀	7.43×10^{-4}	

TABLE 2.2. State Variables

	Meaning
$P(\tau)$	Pathogen concentration at infection-age τ
$M(\tau)$	IgM concentration at infection-age τ
$G(\tau)$	IgG concentration at infection-age τ
$S_H(t)$	Number of susceptible hosts at time t
$i_H(\cdot, t)$	Age-of-infection density of infected hosts at time t
$R_H(t)$	Cumulative number of recovered hosts at time t
$S_V(t)$	Number of susceptible vectors at time t
$I_V(t)$	Number of infected vectors at time t

Next, we highlight the threshold dynamics of the system, including long-term behavior of the solutions, explicit expressions of equilibria and basic reproduction number.

Let us define the *immune-response-dependent reproduction number of the epidemic* as

$$(2.4) \quad \mathcal{R}_0 = \frac{\beta_V S_H^0}{\mu} \int_0^\infty S_V^0 \beta_H(\tau) e^{-\int_0^\tau (\alpha(s) + \kappa(s) + \gamma(s) + d) ds} d\tau,$$

where $S_H^0 = \frac{\Lambda}{d}$ and $S_V^0 = \frac{\eta}{\mu}$. A detailed analysis of our model (2.1)-(2.3) including also vector age-of-infection was presented in [12]. The vector compartments here correspond to the ones in that paper integrated over vector-infection-age and, therefore, all analytical results therein (e.g. threshold conditions) also hold for our present model. In particular, the following results are established for our model:

Theorem 2. *The disease-free equilibrium (DFE) $\mathcal{E}_0 = (S_H^0, 0, 0, S_V^0, 0)$ is locally asymptotically stable if $\mathcal{R}_0 < 1$ and unstable if $\mathcal{R}_0 > 1$.*

This result is actually global for \mathcal{E}_0 :

Theorem 3. *\mathcal{E}_0 is globally asymptotically stable if $\mathcal{R}_0 < 1$ and unstable if $\mathcal{R}_0 > 1$.*

Furthermore, when $\mathcal{R}_0 > 1$, the system (2.2) has a unique endemic equilibrium (EE) $\mathcal{E}^* = (S_H^*, i_H^*(\tau), R_H^*, S_V^*, I_V^*)$ (also presented in [14]), where

$$(2.5) \quad \begin{cases} S_H^* = \left(\beta_V \frac{S_V^*}{\mu} \int_0^\infty \beta_H(\tau) \pi_H(\tau) d\tau \right)^{-1}, \\ i_H^*(\tau) = i_H^*(0) \pi_H(\tau), \\ R_H^* = \frac{i_H^*(0)}{d} \int_0^\infty \gamma(\tau) \pi_H(\tau) d\tau, \end{cases}$$

$$(2.6) \quad \begin{cases} S_V^* = \eta \left(i_H^*(0) \int_0^\infty \beta_H(\tau) \pi_H(\tau) d\tau + \mu \right), \\ I_V^* = \frac{S_V^*}{\mu} \int_0^\infty \beta_H(\tau) i_H^*(\tau) d\tau, \end{cases}$$

with
(2.7)

$$i_H^*(0) = S_0^H \left(1 - \frac{1}{\mathcal{R}_0}\right) / \left(\frac{1}{d} + \frac{\mu}{\beta_V \eta}\right), \quad \pi_H(\tau) = e^{-\int_0^\tau (\alpha(s) + \kappa(s) + \gamma(s) + d) ds},$$

and the epidemiological parameters $\beta(\tau)$, $\gamma(\tau)$, $\alpha(\tau)$, and $\kappa(\tau)$ are given by (2.3). For this equilibrium we have the following results.

Theorem 4. *The endemic equilibrium $\mathcal{E}^* = (S_H^*, i_H^*(\tau), R_H^*, S_V^*, I_V^*)$ is locally asymptotically stable whenever it exists (i.e. for $\mathcal{R}_0 > 1$).*

Theorem 5. *If $\mathcal{R}_0 > 1$, then the disease is uniformly weakly endemic.*

In fact, the global stability of a unique endemic equilibrium is shown in [18] under an equivalent threshold condition to $\mathcal{R}_0 > 1$. These results show that \mathcal{R}_0 represents both a threshold between extinction and persistence and a strict threshold for disease eradication.

3. IMPACT OF IMMUNE PARAMETERS ON EPIDEMIC QUANTITIES

SA of immuno-epidemiological models not only provides a measure of the influence of epidemic parameters on the spread and abundance of the disease at the population scale, but also of those at within-host scale. In particular, SA of immunological parameters on epidemic quantities might provide valuable information on the expected impact of control strategies including those targeted toward: (i) *the host population such as vaccination, and drug treatment*, (ii) *the vector population, such as Wolbachia-based control strategies*, and (iii) *curbing viral production by providing important comparisons of the efficacy of different immune variables*. To determine the impact of immunological parameters on the disease dynamics at population scale, we carry out the SA of the epidemiological quantities \mathcal{R}_0 , I_H^* and I_V^* with respect to the immune model parameters in (2.1). Notice that the prior studies on SA only focus on the impact of *epidemic* parameters on epidemic quantities.

The normalized forward sensitivity index of a quantity of interest (QOI) q to a parameter of interest (POI) p can be defined as the ratio of relative change in the variable to the relative change in the parameter:

$$\gamma_p^q = \frac{\partial q}{\partial p} \times \frac{p}{q}.$$

The baseline parameter values and ranges for RVFD are presented in Table 2.1. The baseline values were fitted to multi-scale data in [23]: for immunological parameter estimations, immunological RVF time-series data was obtained from livestock (in laboratory experiments), and for the epidemiological model, incidence data was acquired from the 2006–2007 Kenya Outbreak [6, 21]. This simultaneous fitting of immunological and epidemiological model parameters induces practical identifiability of model parameters [23].

We first consider the normalized sensitivity index for the basic reproduction number $\gamma_p^{\mathcal{R}_0}$. Note that for consistency regarding parameter estimates in Tuncer et al. [23], we assume that $\Lambda = d$, and $\eta = \mu$, which set the total number of susceptible hosts, S_H^0 , equal to 1 at the DFE, \mathcal{E}_0 .

From (2.4), we have

$$(3.1) \quad \frac{\partial \mathcal{R}_0}{\partial p} = \frac{\beta_V}{\mu} \int_0^\infty \left(\frac{\partial \beta_H(\tau, p)}{\partial p} \pi_H(\tau, p) + \beta_H(\tau, p) \frac{\partial \pi_H(\tau, p)}{\partial p} \right) d\tau,$$

where $\beta_H(\tau, p)$ and $\pi_H(\tau, p)$ are defined in (2.3) and (2.7), respectively, and

$$(3.2) \quad \begin{aligned} \frac{\partial \beta_H(\tau, p)}{\partial p} &= \frac{C_\beta C_0}{(C_0 + P(\tau))^2} \frac{\partial P(\tau, p)}{\partial p}, \\ \frac{\partial \pi_H(\tau, p)}{\partial p} &= -\pi_H(\tau) \int_0^\tau \left(\zeta \frac{\partial P(s, p)}{\partial p} + \xi \frac{\partial M(s, p)}{\partial p} \right. \\ &\quad \left. + C_\gamma \frac{\frac{\partial G(s, p)}{\partial p} (P(s, p) + \epsilon_0) - G(s, p) \frac{\partial P(s, p)}{\partial p}}{(P(s, p) + \epsilon_0)^2} \right) ds. \end{aligned}$$

Note that we need to compute $\frac{\partial \mathbf{x}}{\partial p}(\tau, p)$, where $\mathbf{x}(\tau, p) = (P(\tau, p), M(\tau, p), G(\tau, p))$, the state variables of the within-host model (2.1). From Clairaut's Theorem, we have

$$(3.3) \quad \frac{\partial}{\partial \tau} \left(\frac{\partial \mathbf{x}}{\partial p} \right) = \frac{\partial}{\partial p} \left(\frac{\partial \mathbf{x}}{\partial \tau} \right),$$

where $\partial \mathbf{x} / \partial \tau$ is the right-hand side of the system (2.1). Let $\mathbf{f}(\mathbf{x}, p) = \partial \mathbf{x} / \partial \tau$, and consider the following system for the derivatives $\partial \mathbf{x} / \partial p$:

$$(3.4) \quad \begin{cases} \frac{\partial}{\partial \tau} \left(\frac{\partial \mathbf{x}}{\partial p} \right) = \frac{\partial \mathbf{f}}{\partial \mathbf{x}} \frac{\partial \mathbf{x}}{\partial p} + \frac{\partial \mathbf{f}}{\partial p}, \\ \frac{\partial \mathbf{x}}{\partial p}(0) = \mathbf{0}, \end{cases}$$

where $\partial \mathbf{f} / \partial \mathbf{x}$ is the Jacobian matrix of the right-hand side of the system (2.1). For example, taking parameter $p = a$, the IgM immune response activation rate, we can derive the corresponding system (3.4) as follows

$$\underbrace{\begin{pmatrix} \frac{\partial}{\partial t} \left(\frac{\partial P}{\partial a} \right) \\ \frac{\partial}{\partial t} \left(\frac{\partial M}{\partial a} \right) \\ \frac{\partial}{\partial t} \left(\frac{\partial G}{\partial a} \right) \end{pmatrix}}_{\frac{\partial}{\partial t} \left(\frac{\partial \mathbf{x}}{\partial a} \right)} = \underbrace{\begin{pmatrix} r \left(1 - \frac{2P}{K} \right) - \theta M - \delta G & -\theta P & -\delta P \\ aM & aP - (q + c) & 0 \\ bG & q & bP \end{pmatrix}}_{\frac{\partial \mathbf{f}}{\partial \mathbf{x}}} \underbrace{\begin{pmatrix} \frac{\partial P}{\partial a} \\ \frac{\partial M}{\partial a} \\ \frac{\partial G}{\partial a} \end{pmatrix}}_{\frac{\partial \mathbf{f}}{\partial a}} + \underbrace{\begin{pmatrix} 0 \\ MP \\ 0 \end{pmatrix}}_{\frac{\partial \mathbf{f}}{\partial a}}.$$

By solving the extended system (3.4)-(2.1), we obtain the solutions for \mathbf{x} and the derivatives $\partial \mathbf{x} / \partial p$ at all times τ , which are then utilized to estimate the integrands in (3.1) and (3.2). We then numerically approximate the integrals by using the trapezoidal rule. Note that (3.4) is the standard derivation for the *variational system* of an ODE.

Similarly, we assess the impact of within-host parameters on the final epidemic size, consider the endemic host population size I_H^* and endemic vector population size I_V^* as the QOIs, which are given in (2.5) and (2.6), respectively. The corresponding sensitivity

matrices are derived as follows:

$$\frac{\partial I_H^*}{\partial \mathbf{p}} = \int_0^\infty \left[\frac{\partial i_H^*(0)}{\partial \mathbf{p}} \pi_H(\tau) + i_H^*(0) \frac{\partial \pi_H(\tau)}{\partial \mathbf{p}} \right] d\tau, \quad \frac{\partial i_H^*(0)}{\partial \mathbf{p}} = \frac{1}{\mathcal{R}_0^2} \frac{\partial \mathcal{R}_0}{\partial \mathbf{p}} \left/ \left(\frac{1}{d} + \frac{1}{\beta_V} \right) \right.,$$

$$\frac{\partial I_V^*}{\partial \mathbf{p}} = \frac{1}{(\mathcal{R}_0 S_H^*)^2} \left(\frac{\partial \mathcal{R}_0}{\partial \mathbf{p}} S_H^* - \frac{\mathcal{R}_0}{d} \frac{\partial i_H^*(0)}{\partial \mathbf{p}} \right).$$

In Fig.3.1, the immune-response-dependent epidemiological reproduction number, \mathcal{R}_0 , along with the response curves for the extended SA, $\gamma_{\mathbf{p}}^{\mathcal{R}_0}$, are plotted against the immune parameter values p over a range of values around the baseline estimates. In Fig.3.1(a), the epidemiological threshold \mathcal{R}_0 is a non-monotone function of the within-host pathogen replication rate r and there is a critical pathogen replication rate r_c at which the reproduction number is maximal. We present the resulting sensitivity indices at the baseline parameters in Table 3.3, where the indices are sorted by magnitude. The numerical results suggest that:

- i) At the baseline (estimated) values of within-host immune parameters, the within-host viral growth rate r has the largest impact on \mathcal{R}_0 : 1% increase in r causes 0.6% reduction in \mathcal{R}_0 , 0.8% reduction in final infected host abundance \mathcal{I}_H^* and 0.72% reduction in final infected vector abundance \mathcal{I}_V^* .

In Fig.3.1, the reduction in \mathcal{R}_0 with increasing within-host pathogen growth rate r is counter-intuitive, but well known in the literature [1]. The trade-off between pathogen virulence and infectiousness is first shown in [11], articulated through a within-host model for directly transmitted diseases. Later it was extended to vector-borne diseases in [14]. In particular, the reduction in \mathcal{R}_0 for large r occurs due to three mechanisms: (i) death due to “aggressive” immune response, (ii) death due to pathogen exploitation of target cells, and (iii) decreasing infectious period due to large viral clearance. As the pathogen growth increases rapidly, the immune response becomes more robust (See Fig. A.2). Both cases can lead to rapid death of the host, shortening the infectious period, and subsequently leading to a reduction in the average number of secondary cases caused by these infectious individuals. In addition, note that a 1% increase in within-host pathogen growth rate r in the parameter region $r \in [0.1, 2]$ leads to up to 8% increase in \mathcal{R}_0 (Fig.3.1), 1% increase in \mathcal{I}_H^* (Fig.3.2), and 1.5% increase in \mathcal{I}_V^* (Fig.A.4), which are significant increases in population-scale disease quantities, suggesting that control strategies should be targeted toward reducing within-host pathogen growth rate to significantly change the disease outcomes in the long term. For example, within-host pathogen growth rate r can be reduced by immunizing the host population, or through drug treatment during outbreaks, hampering viral growth within-hosts.

- ii) The within-host pathogen carrying capacity K has the second largest impact on \mathcal{R}_0 at the baseline parameter value $K = 7.57 \times 10^7$: 1% increase in K causes 0.079% reduction in \mathcal{R}_0 , 0.060% reduction in \mathcal{I}_H^* , and 0.095% reduction in \mathcal{I}_V^* .
- iii) The within-host IgM immune activation rate a has the third largest impact on \mathcal{R}_0 at the baseline parameter value $a = 1.1 \times 10^{-7}$: 1% increase in a causes 0.019% reduction in \mathcal{R}_0 , 0.015% reduction in \mathcal{I}_H^* , and 0.023% in \mathcal{I}_V^* .

The faster the IgM antibodies activate, the faster they clear the pathogen, causing reduction in disease transmission (See Fig.3.1(c)). A drastic decrease in \mathcal{R}_0 for large values of a suggests that a large improvement in vaccine efficacy is needed for efficient reduction of population-scale transmission.

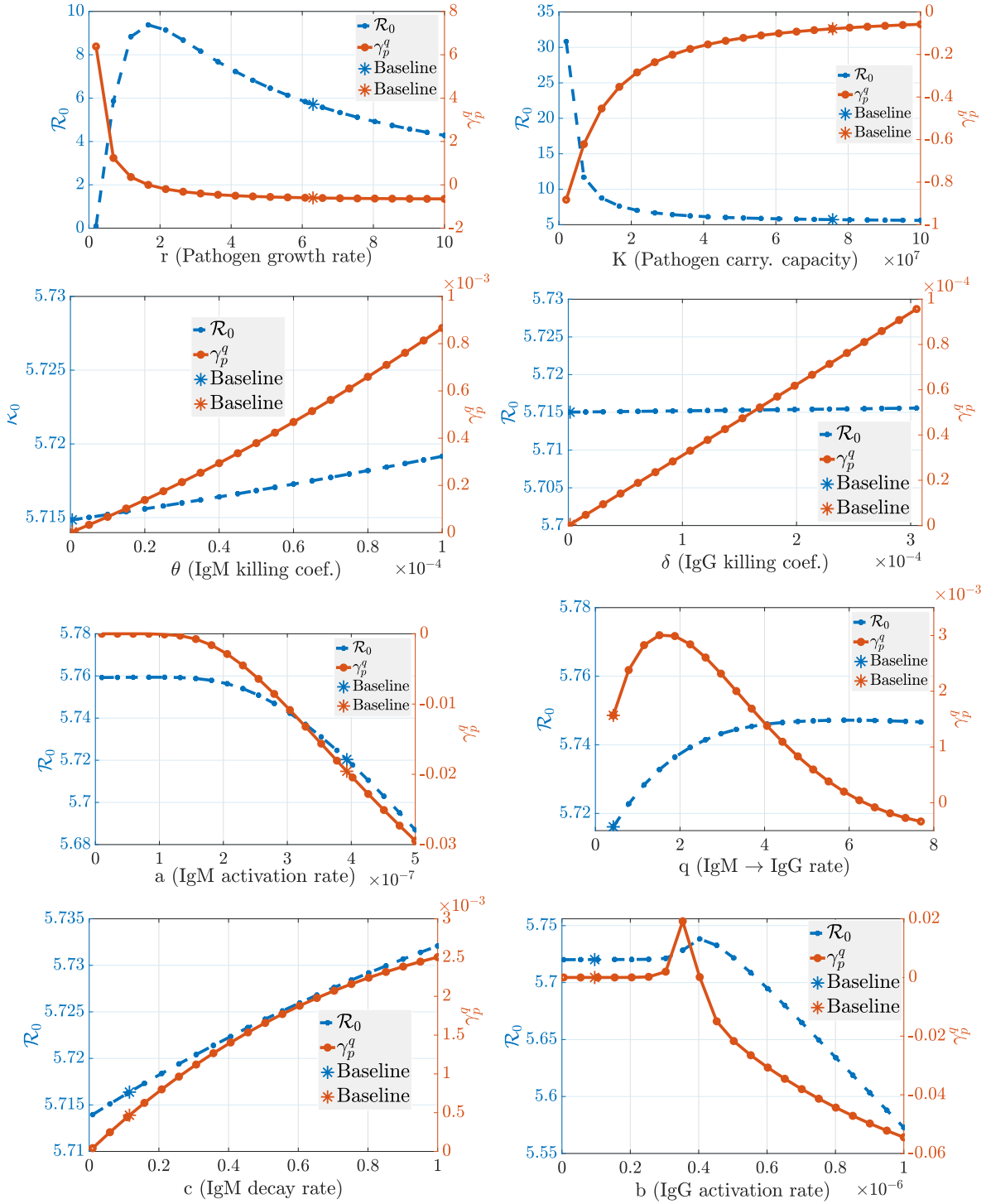


FIGURE 3.1. Impact of immune parameters on the epidemic threshold, \mathcal{R}_0 . The immune-response-dependent epidemiological reproduction number, \mathcal{R}_0 (left y-axis, blue dotted curve) along with the response curves for the extended SA, γ_p^q (right y-axis, orange curve) are plotted against the immune parameter values p over a range of values around the baseline estimates.

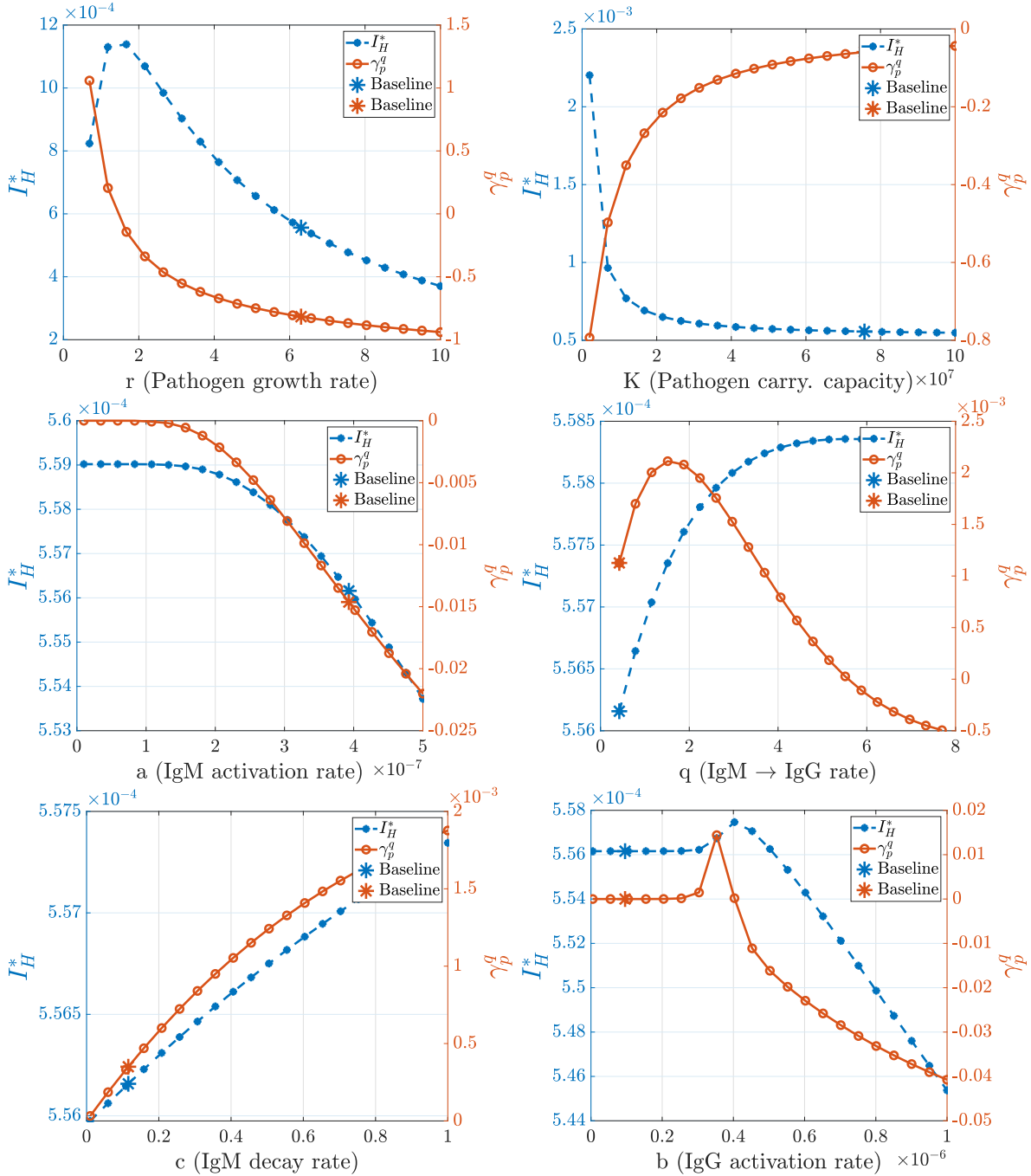


FIGURE 3.2. *Impact of immune parameters on the final epidemic size, \mathcal{I}_H^* . The final infected host disease abundance, \mathcal{I}_H^* , along with the response curves for the extended SA, $\gamma_p^{\mathcal{R}_0}$, are plotted against the immune parameter values p over a range of values around the baseline estimates.*

- iv) The immune response switching rate q has the fourth largest impact on the epidemic quantities, albeit almost negligible: a 1% increase in q causes $1.6 \times 10^{-3}\%$ increase in \mathcal{R}_0 , a $1.13 \times 10^{-3}\%$ increase in \mathcal{I}_H^* and $1.9 \times 10^{-3}\%$ increase in \mathcal{I}_V^* .

TABLE 3.1. Different linking parameter formulations

Definition	Param.	LP ₁	Ref.	LP ₂	Ref.
Host transmission rate	$\beta_H(\tau)$	$\frac{C_\beta P(\tau)}{C_0 + P(\tau)}$	[23]	$\frac{C_\beta^* P^2(\tau)}{(C_0^*)^2 + P^2(\tau)}$	[14]
Pathogen induced death rate	$\alpha(\tau)$	$\zeta P(\tau)$	[23]	$r\zeta^* P(\tau)$	[14, 11]
Antibody induced death rate	$\kappa(\tau)$	$\xi M(\tau)$	[23]	$a\xi^* M(\tau)P(\tau)$	[14, 11]
Host recovery rate	$\gamma(\tau)$	$C_\gamma \frac{G(\tau)}{P(\tau) + \epsilon_0}$	[23]	$C_\gamma^* \frac{G(\tau)}{P(\tau) + \epsilon_0^*} e^{-P(\tau)/P(0)}$	[14]

These numbers suggest that it might be more favorable for the host population if the loss term due to B-cells switching production of IgM antibodies to IgG antibodies (with a per-capita rate q) is smaller. In other words, because the IgM immune response antibodies are mainly responsible for *rapid destruction of virus*, for better outcome in disease eradication, rapid destruction of virus within hosts can be more crucial than the life-long immunity (memory) provided by IgG antibodies.

- v) The IgM immune response decay rate is the next most influential parameter impacting epidemic quantities: a 1% increase in c causes a negligible $4.6 \times 10^{-4}\%$ increase in \mathcal{R}_0 , a $3.5 \times 10^{-4}\%$ increase in \mathcal{I}_H^* , and a $5.6 \times 10^{-4}\%$ increase in \mathcal{I}_V^* .
- vi) Finally, the killing efficacy parameters θ, δ for both immune responses appear to be least impactful immunological parameters.

It is interesting to note that an increase in the killing efficacy parameters can lead to an increase in epidemic quantities, although just marginally. The biological insight behind this numerical observation is that: *because the baseline parameters are in the high disease fatality parameter region, an increase in parameter killing efficacy slows down the viral density growth within-hosts, decreasing disease induced death rates; subsequently, allowing an increase in infectious period, which leads an increase in epidemic quantities (see Fig.A.2 (bottom row subfigures))*. In summary, comparing the impact of immune response parameters, the IgG immune activation rate seems to be the least crucial, underscoring the importance of IgM immune parameters in disease eradication over IgG immune response. However this result might be an artifact of how the disease-induced death rate κ is formulated and what the range of the parameter θ is. We observed that the value of the IgM killing efficacy parameter largely determines the peak viral load in such a way that, when the IgM killing efficacy is chosen sufficiently large, not only the viral relapse occurs but also there is a larger change in the virus density (see the Fig A.3). Since the values of θ in the chosen range are small, we observe no viral relapse and a smaller impact on the viral dynamics, but a larger reduction in the antibody response dynamics.

3.1. The impact of the choice of linking parameters on the SA. An important question is, *how does the choice of linking functions affect the outcome of the SA performed in Section 3?* To study this question, we consider different linking functions that have been implemented in the literature (Table (3.1)), and we carry out the corresponding SA using a similar process to that described in Section 3. To do that we first

TABLE 3.2. Re-calibrated parameters for the alternative linking functions (LP_2) in Table 3.1. The parameters are estimated using nonlinear least squares to match the basic reproduction number \mathcal{R}_0 .

	Linking function parameters	Dimension	Estimated	Range
C_β^*	transmission efficiency ($= C_\beta$)	(host \times day) $^{-1}$	0.5365	-
C_0^*	half saturation in transmission rate	TCID ₅₀	3.030×10^3	$10^3 \sim 10^4$
ζ^*	the pathogen cost coefficient	(TCID ₅₀) $^{-1}$	9.840×10^{-9}	$10^{-9} \sim 10^{-7}$
ξ^*	the immune response cost coefficient	(Elisa PP) $^{-1}$	2.951×10^{-6}	$10^{-7} \sim 10^{-5}$
C_γ^*	recovery coefficient	$\frac{\text{TCID}_{50}}{\text{Elisa PP} \times \text{day}}$	4.860	$0 \sim 10$
ϵ_0^*	half saturation in recovery rate ($= \epsilon_0$)	TCID ₅₀	7.43×10^{-4}	-

TABLE 3.3. Local sensitivity indices $\gamma_{\mathbf{p}}^{QOI}$ with respect to model parameters

LP ₁	$\gamma_{\mathbf{p}}^{\mathcal{R}_0}$	$\gamma_{\mathbf{p}}^{\mathcal{I}_H^*}$	$\gamma_{\mathbf{p}}^{\mathcal{I}_V^*}$	LP ₂	$\gamma_{\mathbf{p}}^{\mathcal{R}_0}$	$\gamma_{\mathbf{p}}^{\mathcal{I}_H^*}$	$\gamma_{\mathbf{p}}^{\mathcal{I}_V^*}$
r	-0.598	-0.817	-0.720	r	-0.7520	-0.925	-0.906
K	-0.0789	-0.0595	-0.0950	K	-0.0801	-0.0607	-0.0964
a	-0.0194	-0.0146	-0.0234	a	-0.0205	-0.0155	-0.0247
q	1.56×10^{-3}	1.13×10^{-3}	1.88×10^{-3}	q	1.64×10^{-3}	1.22×10^{-3}	1.97×10^{-3}
c	4.64×10^{-4}	3.50×10^{-4}	5.59×10^{-4}	c	4.61×10^{-4}	3.49×10^{-4}	5.54×10^{-4}
θ	3.19×10^{-6}	2.40×10^{-6}	3.84×10^{-6}	θ	5.44×10^{-6}	4.12×10^{-6}	6.55×10^{-6}
δ	4.65×10^{-7}	4.39×10^{-7}	5.60×10^{-7}	δ	6.12×10^{-7}	5.50×10^{-7}	7.37×10^{-7}
b	3.10×10^{-7}	2.31×10^{-7}	3.74×10^{-7}	b	4.21×10^{-7}	3.18×10^{-7}	5.07×10^{-7}

TABLE 3.4. Local epidemic sensitivity indices $\gamma_{\mathbf{p}}^{\mathbf{q}}$ with respect to within-host model parameters.

<i>Fatal</i>	$\gamma_{\mathbf{p}}^{\mathcal{R}_0}$	<i>Mild</i>	$\gamma_{\mathbf{p}}^{\mathcal{R}_0}$
r	-0.598	r	0.587
K	-0.0789	K	-0.0137
a	-0.0194	a	-0.0029
q	1.56×10^{-3}	q	-0.00193
c	4.64×10^{-4}	c	5.54×10^{-4}
θ	3.19×10^{-6}	b	4.91×10^{-7}
δ	4.65×10^{-7}	θ	3.88×10^{-7}
b	3.10×10^{-7}	δ	-3.65×10^{-7}

re-calibrate the coefficients in the alternative linking functions (LP_2 -columns in Table 3.1) by solving the following optimization problem:

$$\min_{C^* \in (C_L, C_R)} |\mathcal{R}_0(C^*) - \mathcal{R}_0|,$$

to approximate the basic reproduction number \mathcal{R}_0 at the baseline setting. We have fit the four linking parameters, $C_0^*, \zeta^*, \xi^*, C_\gamma^*$, one at a time: we vary one linking parameter C^* over its corresponding range, (C_L, C_R) , specified in Table 3.2, while keeping all the other parameters in the LP_1 forms at their baseline values. This single-variable optimization was repeated for each of the four linking parameters, and it was done using the `fminbnd` algorithm in MATLAB with `TolX` = 10^{-10} . The resulting estimates are listed in Table 3.2.

We present the resulting sensitivity indices for these new linking functions in Table 3.3 (LP_2 columns). Comparing these with the indices for the original linking functions (LP_1 columns), we see the same ordering by magnitude and comparable values for different the paired linking functions. The numerical results suggest that the choice of linking functions, after fitting their linking parameters at the baseline values of the immunological and epidemiological parameters from Tuncer et. al.[23], does not cause important differences in \mathcal{R}_0 -values (Fig.A.5). We also observe similar patterns in the corresponding curves for final disease abundance I_H^* and I_V^* (Appendix A.2).

Furthermore, notice that at the baseline (estimated) parameter values, we have $\partial\mathcal{R}_0/\partial r < 0$ due to increasing disease induced fatality and decreasing infectious period. Therefore, we classify the diseases according to different ranges of r as: *fatal* when $\partial\mathcal{R}_0/\partial r < 0$; *mild* if $\partial\mathcal{R}_0/\partial r > 0$. Then, independently of the choice of linking functions, we obtain that when the disease is fatal:

- The within-host pathogen growth rate r , and pathogen carrying capacity K have the largest impact on the disease reproduction number and final disease abundance size, suggesting that the most efficient control measures are the ones that target reducing within-host viral growth rate, even if virus eradication within hosts cannot succeed.
- Compared to IgG immune response, the IgM immune response parameters have larger impact on the disease outcomes.
- Changes in the host immune response parameters have a larger impact on the final infected vector abundance (I_V^*) than on the final infected host abundance (I_H^*) because of the indirect transmission route.

Next we consider the parameter region, where the disease is mild by fixing $r = 1$. For this case, we observe that SA of QOI to the within-host parameters r, q and δ change signs, and the order of the sensitivity indices by magnitude is slightly different, suggesting that:

- Independently of disease fatality, the per capita parasite growth rate consistently appears to be the most important within-host parameter impacting disease spread. Yet in the mild case (as opposed to fatal case):1% increase in r causes 0.587% increase in \mathcal{R}_0 , i.e. increasing the final disease abundance.
- However 1% increase in carrying capacity K causes 0.0137% reduction in \mathcal{R}_0 . This reduction also holds when r is in the “fatal” parameter region. The biological insight behind this finding is that an increase in within-host pathogen carrying

capacity causes the host to harbor more pathogens, resulting in increased fatality due to pathogen resource use.

- An increase in the immune-response activation rates decreases the epidemic quantities. Yet, IgM parameters, compared to IgG, still appear to be more impactful. This suggests that vaccine efficacy can be tested by measuring the increase in IgM and IgG antibody densities comparing data pre- and post-vaccination.

However, in the mild case, other parameters may also see a change in their baseline values corresponding to changing values of r because the parameters in the model may not be independent from each other. For a more rigorous comparison of the mild and the fatal cases, one needs to have another data set representing the mild disease, and fit other parameters as well, which we suggest as valuable future work.

3.2. Impact of viral replication rate on infectability during distinct phases of infection and epidemic.

So far we focused on the impact of immune parameters on the basic reproduction number \mathcal{R}_0 and the steady state infected host, I_H^* , and infected vector abundance I_v^* . Next, we will show how *infectability* sensitivity with respect to key immune parameters, $\gamma_{\mathbf{p}}^{\beta(\tau)i_H(\tau,t)}$ (derived in Appendix A.3), during different outbreak phases and (within-host) infection-times shows heterogeneous impact of virulence-transmission trade-off. Recall that the *normalized forward sensitivity index* $\gamma_{\mathbf{p}}^{\beta(\tau)i_H(\tau,t)}$ quantifies *how much the infectability of cohort of individuals $i_H(\tau,t)$ changes when the parameter \mathbf{p} is increased by 1%*. In contrast to the reproduction number and steady states, infectability, defined with the epidemic quantity $\beta(\tau)i_H(\tau,t)$, is a function of times since outbreak and individual infection start, t and τ , respectively, allowing us to see within-host effect on the main population level determinant of force of infection which varies with t and τ . Although sensitivities are calculated for all immune parameters, because the viral replication rate is the fastest evolving parameter determining virulence [11, 14], we highlight here the influence of r on infectability, dependent on both infection-age of cohorts of infected individuals and time since outbreak began on population scale (see Appendix A.3 for other parameter sensitivities and additional figures). In this way we can understand how, in general, a virus might evolve in response to control strategies acting at different epidemic phase and different times during infection course (e.g. isolation of infected cases), or conversely how interventions may be optimally timed given the viral replication rate.

We observe in Fig.3.3 and Fig.A.8(a) that the raw (non-normalized) sensitivity of infectability to viral replication rate, $(\beta \times i_H)_r(\tau,t)$, is positive during early infection (small τ) and negative after a sufficient amount of time-since infection passes, and the magnitude amplifies at later phases of the epidemic. Indeed, increasing r causes the within-host infection to be more severe and acute, with larger and earlier peaks of both virus and immune response, thereby tending to shift the transmissions caused by an infected individual to occur earlier during infectious period. Certain control strategies, such as contact tracing, self-isolation, case finding and hospitalization, require some time τ after infection to act due to delays in symptom onset or tracking, and thus the increased transmissibility during early infection of viral strains with higher r values may make these interventions harder to implement [3, 4, 17]. In this way, a virus may tend to evolve larger replication rates in response to these control strategies, which may increase disease virulence. With this knowledge, public health authorities may prioritize rapid

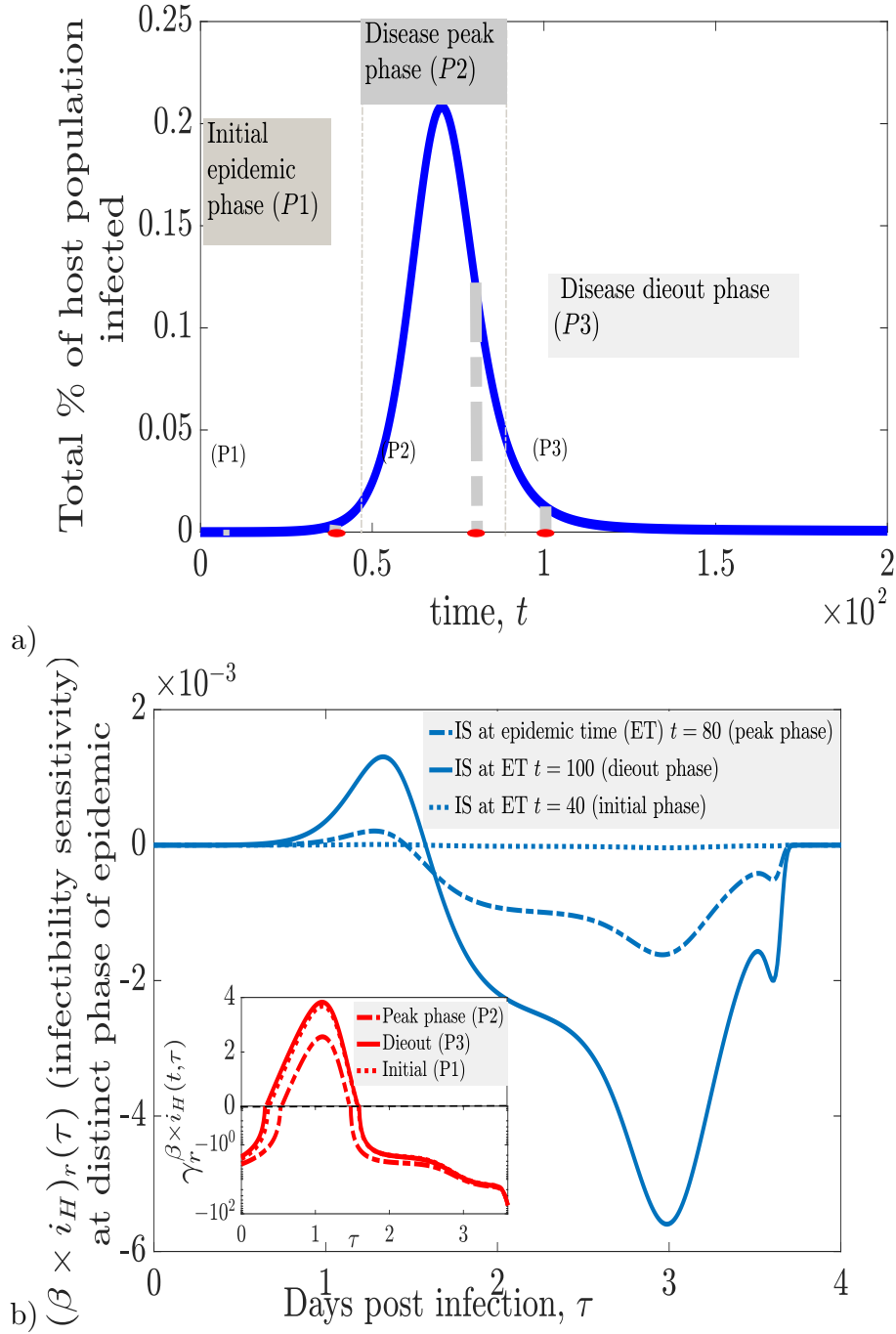


FIGURE 3.3. Sensitivity of infectability of host (at distinct epidemic phase at time t) to viral replication rate r .

response for active and passive case finding in order to combat evolution of and existent virulent strains.

Furthermore, Fig.3.3 suggests that the change in viral replication rate can impact the infection transmissibility of individuals differently depending on epidemic phase. In particular, in the inset figure in Fig.3.3(b), we observe that when within-host parasite

growth rate is increased by 1%, infection transmissibility increases up to 4% at epidemic time $t = 40$ (initial epidemic phase) and at $t = 100$ (epidemic die out phase), but only up to 2.5% during epidemic peak phase ($t = 80$), with the maximum increase occurring around 1 day post infection and almost 100% decrease in transmissibility during the end of infection because of the more acute infection. This normalized sensitivity and the raw sensitivities show that varying r may dramatically shift infectability to earlier infection ages at the later declining phase of epidemic, making the implications of virulence and control strategies discussed in previous paragraph even more relevant. Note that these results might be due to estimated parameters values for RFVD. More rigorous assessment of immune parameters on the infection transmissibility requires further developed techniques in fitting data from within-host and between-host scales to immuno-epidemiological models.

4. DISCUSSION

There are some good reasons for the use of SA in immuno-epidemiological models. First, infectious diseases operates at both immunological (individual) and epidemiological (population) scales. Therefore, quantifying how the underlying immunological processes affect the dynamics of the epidemic can be naturally approached by SA of multi-scale systems. Secondly, SA of epidemic models is frequently used to assess the impact of control strategies that impact the within-host (or in-vector) virus-and-immune-response dynamics, such as vaccination, drug treatment or bio-control strategies (e.g. Wolbachia-based). A rigorous approach of SA requires the assessment of the sensitivity of epidemic quantities to immunological parameters. Finally, since obtaining population scale data is a challenging task and requires costly surveillance efforts, the parameters estimated from within-host viral and immune-response data that can be obtained less costly from laboratory experiments, can be helpful for control strategy development and its assessment. Therefore, to investigate how within-host immune parameters affect disease spread among host population, the SA of the multi-scale models, as the one introduced here, can be informative and give crucial insights on the expected impact of control strategies and their efficacy.

Our results suggest that the within-host per capita parasite growth rate r has the largest impact on disease spread: *1% increase in r in the parameter region $r \in [0.1, 2]$ leads to up to 8% increase in \mathcal{R}_0 , and up to 1% increase in \mathcal{I}_H^* , and 1.5% increase in \mathcal{I}_V^* , which are significant numbers concerning disease outcomes.* Among the rest of the within-host immune parameters none has a significant impact on the epidemic at the population scale. We may still note that, IgM immune response (mainly responsible for the initial rapid destruction of virus within the host) parameters have larger impact compared to those of IgG immune response (responsible for life-long immunity). When the disease is fatal, a 1% increase in q (IgM \rightarrow IgG switching rate) leads to an increase in \mathcal{R}_0 and when it is mild, it decreases the epidemic quantities. This suggests that when the disease is mild, it is more favorable for the host population to have more IgG antibodies that provide life-long immunity. On the other hand, when the disease is fatal, it emphasizes the benefit of a smaller switching rate. Interestingly, increases in the IgM or IgG virus killing efficacy parameters θ , and σ (respectively), both lead to increases in \mathcal{R}_0 , albeit insignificant ones.

In previous studies [14, 11, 23], the choice of linking epidemic parameters as functions of immune variables were different. Therefore to address how sensitivity indices, $\gamma_{\mathbf{p}}$, change with respect to linking functions chosen, we first non-dimensionalize all linking functions, and then fit the unknown parameters in them using data from prior studies. By doing so, we show that the different linking functions considered do not cause differences in the main outcomes of SA of immunological parameters on epidemic quantities. An interesting numerical result is that even though the unknown parameters in linking functions are fitted at the baseline (estimated) parameters, the consistency on the overlapping parameter values continues over a range of parameter values given as nontrivial intervals around those baseline values.

SA is a common methodological approach to determine the impact of model parameters on the within- and between-host population dynamics quantities. However, these two scales are typically treated separately. Since infectious diseases operate at both scales, in order to understand the crucial mechanisms behind disease dynamics and the impact of targeted control strategies, we need the formulation and analysis of unified models describing disease progression on both scales. One of the biggest challenges for using immuno-epidemiological models is the lack of multi-scale parameter estimations. The sensitivity analysis approach described here is local in nature. Generally, the sensitivity near one choice of parameter values maybe very different from that near a different choice of parameter values, so that a separate sensitivity analysis would need to be performed for every different choice of baseline parameters. However, for the system at hand, we based our parameter estimates on [23], where it was shown that the model is globally structurally identifiable; that is, a unique set of parameters produces the best fit to the data. Therefore, the fitted parameter estimates we use are reliable.

Finally, the model introduced here can be reformulated to incorporate seasonality and temperature-dependent vector growth cycle and vertical transmission in the mosquito population. We plan to extend the present model in the future by incorporating these mechanisms to investigate the impact of seasonality and temperature-dependent vector growth cycle along together with within-host immunological parameters on the disease dynamics at population scale. This might enable us to forecast the impact of implemented control strategies and inform changes to increase their efficacy to help reduce or eradicate the disease. Even though not a vector-host disease, we may also extrapolate implications to the COVID-19 pandemic. In the presence of unprecedented control efforts which included intensive case finding, COVID-19 evolved more virulent variants, such as the Delta variant, which rapidly spread in some countries that were in declining phases of epidemic waves. This evolution of increased viral replication rate contrasts some previous theory that viruses might evolve to be less virulent, and suggest that closer consideration of multi-scale infection-age models may be important to understand virulence-transmission trade-offs and evolution.

5. APPENDIX

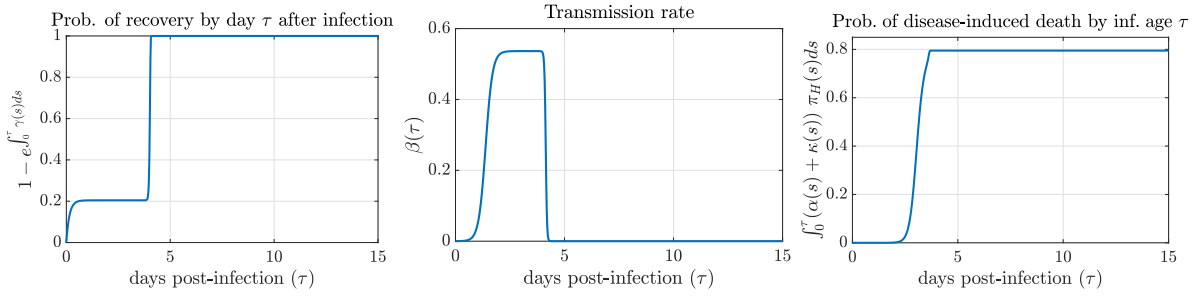


FIGURE A.1. *The evolution of epidemiological parameters over the course of infection w.r.t. days post infection τ . a) Probability of the host being recovered at infection age τ , given that infectious hosts can exit the infected compartment only through recovery. b) Transmission rate w.r.t. the infection age τ . c) Probability of death occurring due to disease by infection age τ . Parameter values are given in Table 2.1 and the corresponding within-host dynamics is displayed in the right subfigure of Fig.2.1.*

A.1. **SA curves for final infected vector abundance, \mathcal{I}_V^*** . See Fig. A.4

A.2. **Impact of using different linking functions on SA: \mathcal{I}_H^* and \mathcal{I}_V^*** . See Fig. A.6 and Fig. A.7.

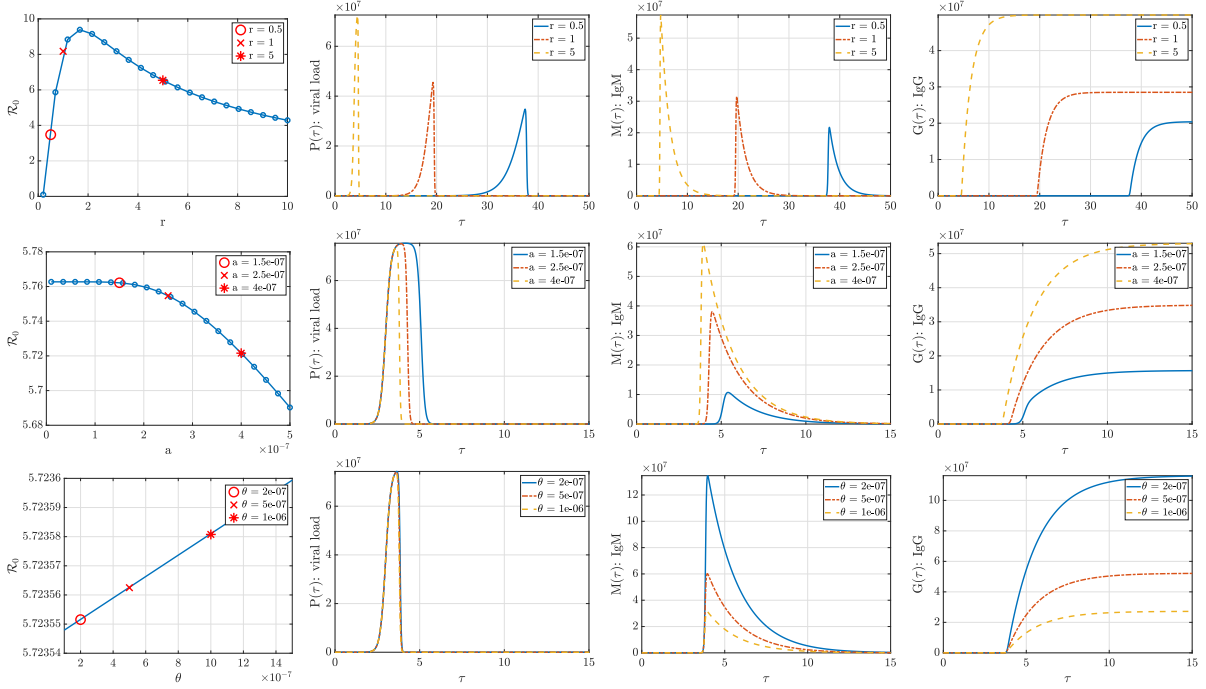


FIGURE A.2. **Top row:** \mathcal{R}_0 vs. pathogen growth rate r . As pathogen growth rate r increases, the infectious period decreases with larger peak load and the immune response antibodies become more prevalent. **Middle row:** \mathcal{R}_0 vs. IgM activation rate a . The faster the IgM antibodies activate, the faster they clear the pathogen with smaller peak load and decreasing infectious period. **Bottom row:** \mathcal{R}_0 vs. killing efficiency of IgM θ . As the immune response triggered by IgM antibodies become more efficient at killing pathogens, the pathogen load and subsequent immune response get smaller.

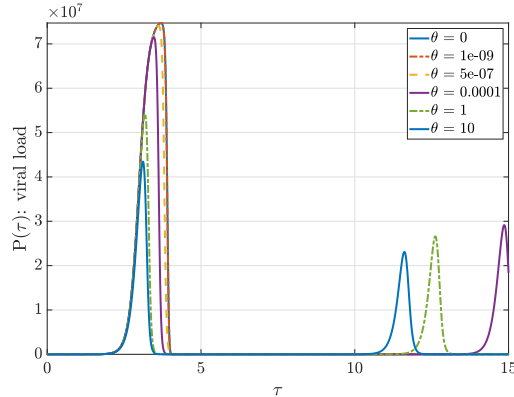


FIGURE A.3. Impact of killing efficacy θ on the viral dynamics.

A.3. Derivation of infectability Sensitivity Matrix. By utilizing Clairaut's theorem, we first obtain the derivative of the system (2.2) with respect to a model parameter

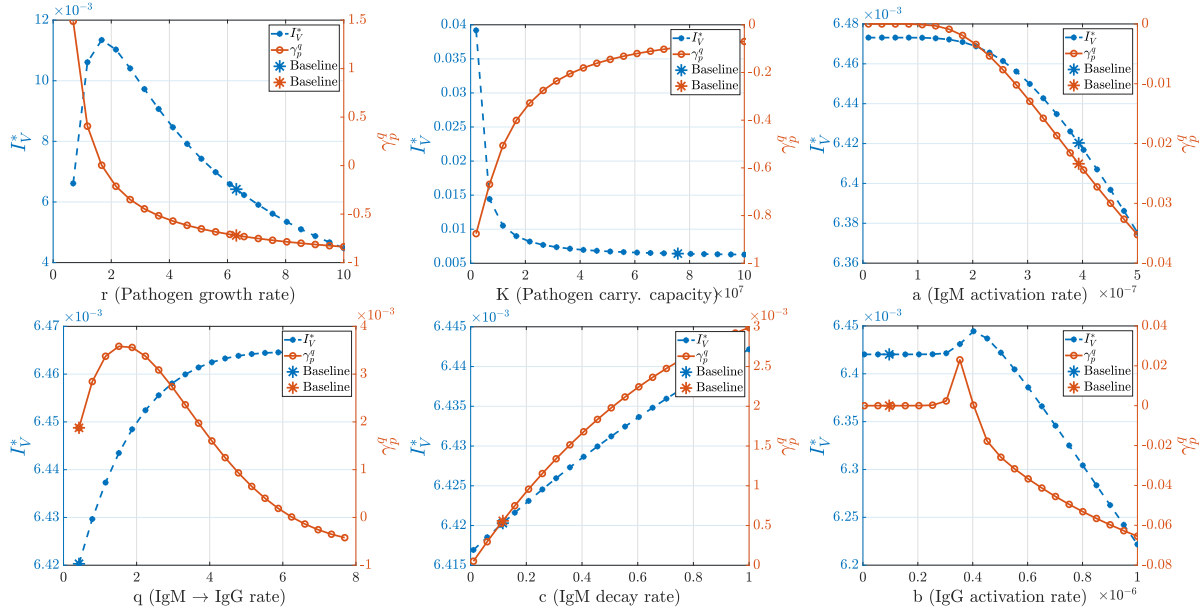


FIGURE A.4. Impact of immune parameters on the steady-state infected vector abundance, \mathcal{I}_V^* . Notice that numerical results for SA for vector component are similar to SA of \mathcal{R}_0 , and the steady-state host endemic size \mathcal{I}_H^* .

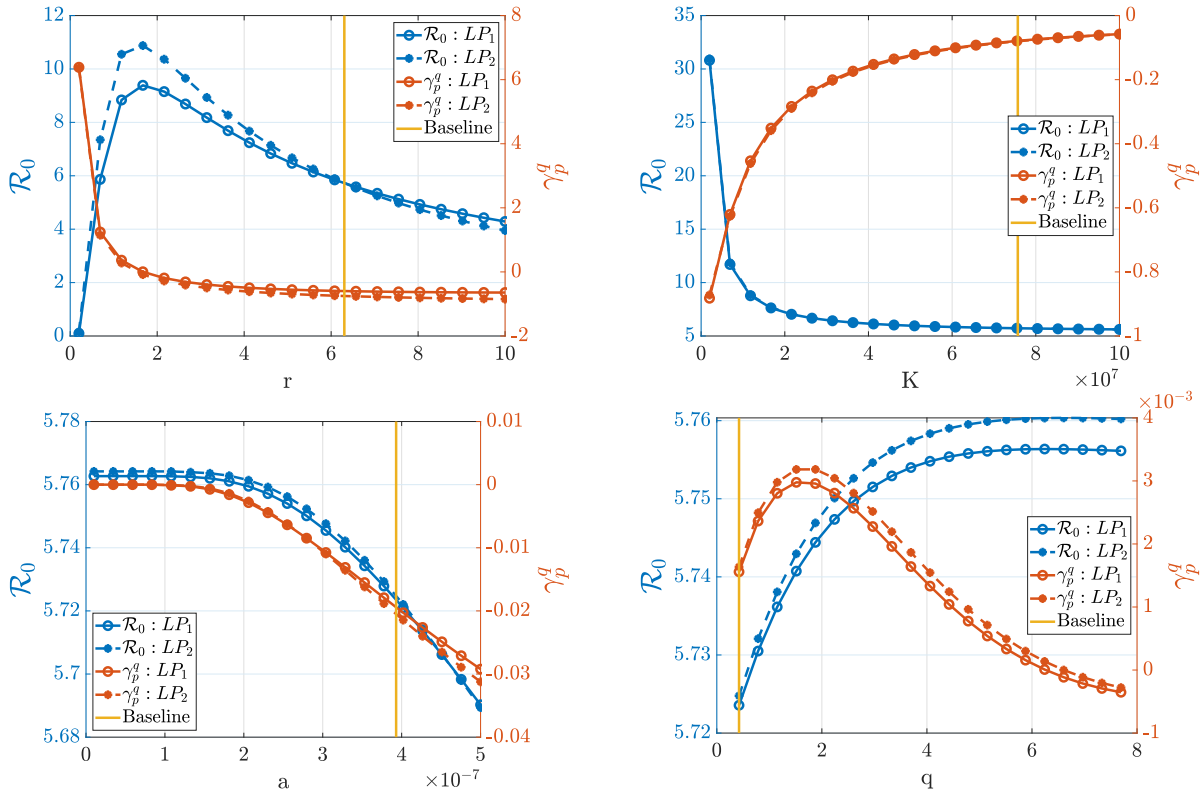


FIGURE A.5. Impact of the choice of linking functions on the SA.

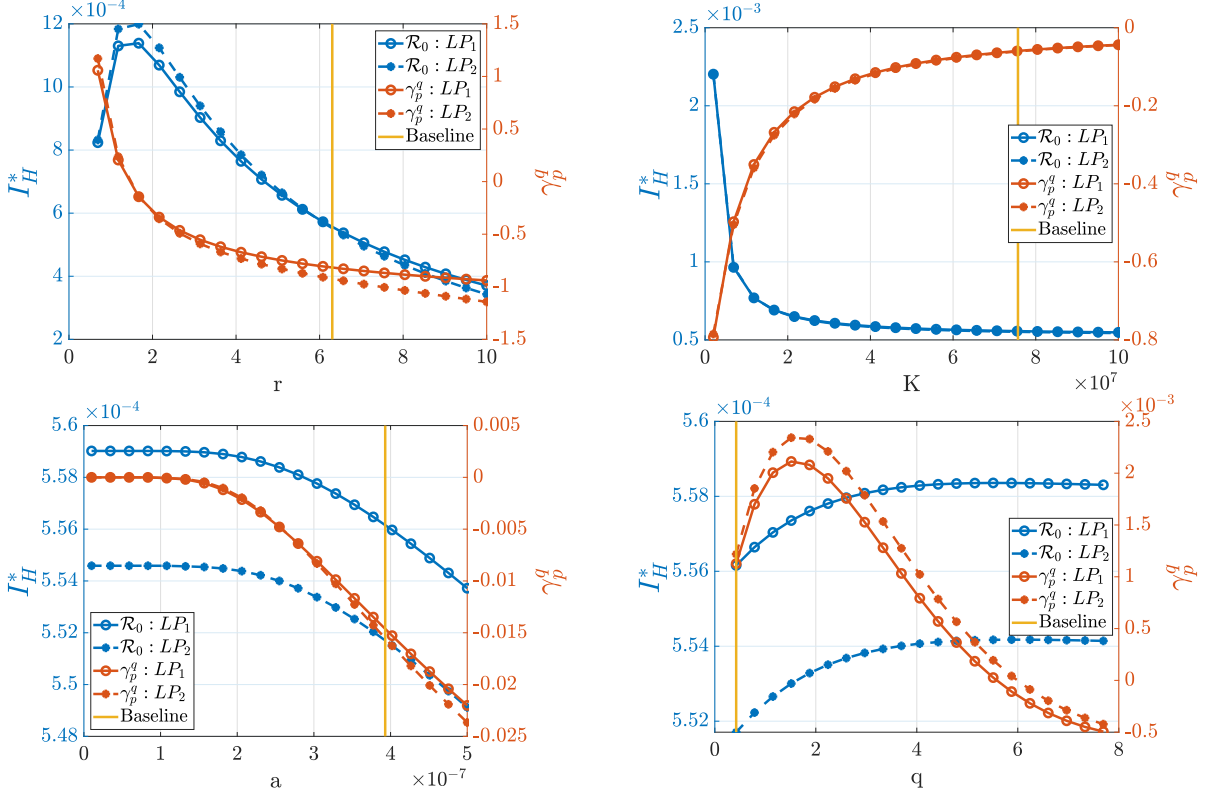


FIGURE A.6. Impact of the choice of linking functions on the SA.

p :

(A.1)

$$\begin{aligned} \frac{\partial}{\partial t} \left(\frac{\partial S_H}{\partial p} \right) &= -\beta_V \frac{\partial S_H}{\partial p} I_V(t) - \beta_V S_H(t) \frac{\partial I_V}{\partial p} - d \frac{\partial S_H}{\partial p} \\ \frac{\partial}{\partial t} \left(\frac{\partial i_H}{\partial p} \right) + \frac{\partial}{\partial \tau} \left(\frac{\partial i_H}{\partial p} \right) &= -\frac{\partial ((\alpha(\tau) + \kappa(\tau) + \gamma(\tau) + d))}{\partial p} i_H(\tau, t) - (\alpha(\tau) + \kappa(\tau) + \gamma(\tau) + d) \left(\frac{\partial i_H}{\partial p} \right), \\ \frac{\partial i_H(0, t)}{\partial p} &= \beta_V \frac{\partial S_H}{\partial p} I_V(t) + \beta_V S_H(t) \frac{\partial I_V}{\partial p}, \\ \frac{\partial}{\partial t} \left(\frac{\partial R_H}{\partial p} \right) &= \int_0^\infty \left(\frac{\partial \gamma(\tau)}{\partial p} i_H(\tau, t) + \gamma(\tau) \frac{\partial i_H(\tau, t)}{\partial p} \right) d\tau - d \frac{\partial R_H}{\partial p}, \\ \frac{\partial}{\partial t} \left(\frac{\partial S_V}{\partial p} \right) &= -\frac{\partial S_V}{\partial p} \int_0^\infty \beta_H(\tau) i_H(\tau, t) d\tau - S_V(t) \int_0^\infty \left(\frac{\partial \beta_H}{\partial p} i_H(\tau, t) + \beta_H(\tau) \frac{\partial i_H(\tau, t)}{\partial p} \right) d\tau - \mu \frac{\partial S_V}{\partial p}, \\ \frac{\partial}{\partial t} \left(\frac{\partial I_V}{\partial p} \right) &= \frac{\partial S_V}{\partial p} \int_0^\infty \beta_H(\tau) i_H(\tau, t) d\tau + S_V(t) \int_0^\infty \left(\frac{\partial \beta_H}{\partial p} i_H(\tau, t) + \beta_H(\tau) \frac{\partial i_H(\tau, t)}{\partial p} \right) d\tau - \mu \frac{\partial I_V}{\partial p}. \end{aligned}$$

Following the numerical scheme in [23], we discretize the system using the Backward Euler difference quotient along the characteristic, and obtain the following fully-discretized

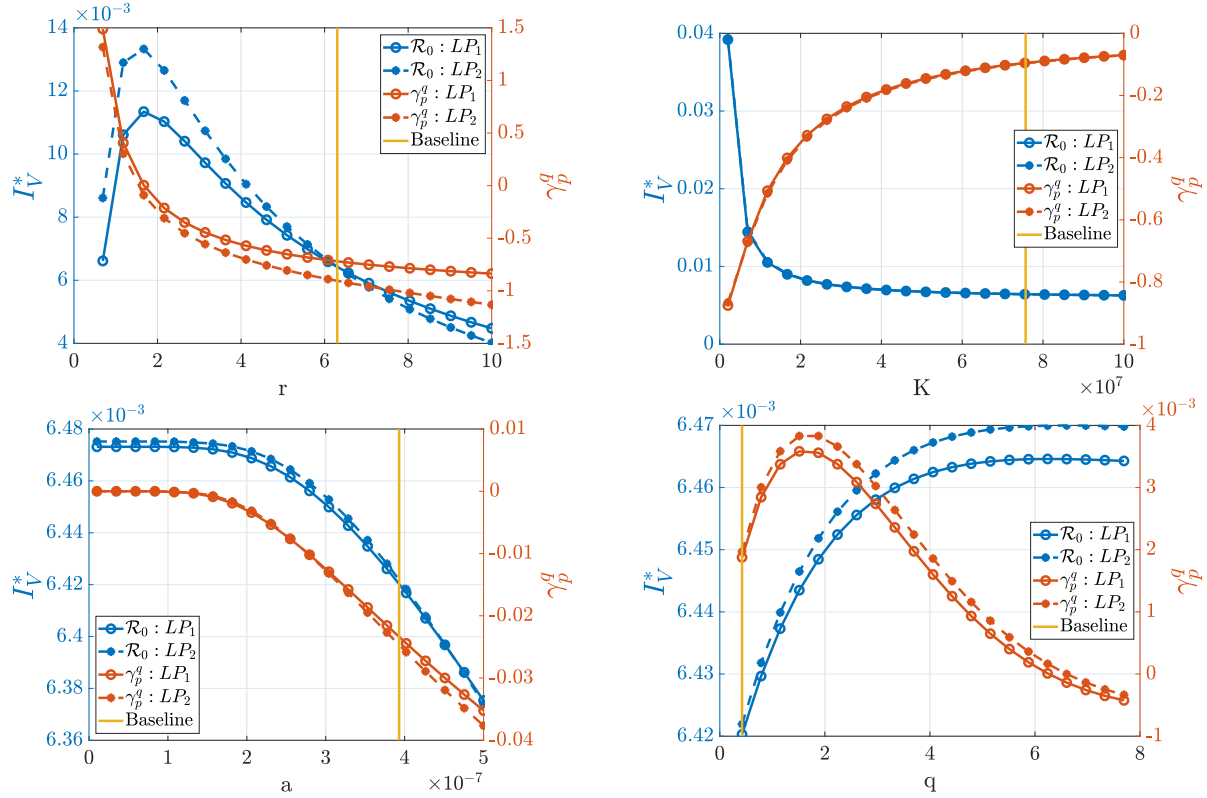


FIGURE A.7. Impact of the choice of linking functions on the SA.

finite difference scheme:

$$(A.2) \quad \left\{ \begin{array}{l} \frac{S_H^{n+1} - S_H^n}{\Delta t} = \Lambda - \beta_v S_H^{n+1} I_v^n - d S_H^{n+1}, \quad \frac{i_H^{k+1,n+1} - i_H^{k,n}}{\Delta t} = -(\alpha_{k+1} + \gamma_{k+1} + d) i_H^{k+1,n+1}, \\ i_H^{0,n+1} = \beta_v S_H^{n+1} I_v^{n+1}, \\ \frac{S_v^{n+1} - S_v^n}{\Delta t} = \eta - S_v^{n+1} \sum_{k=1}^M \beta_H^k i_H^{k,n+1} - \mu S_v^{n+1}, \quad \frac{I_v^{n+1} - I_v^n}{\Delta t} = S_v^{n+1} \sum_{k=1}^M \beta_H^k i_H^{k,n+1} - \mu I_v^{n+1} \\ \frac{S_{H_p}^{n+1} - S_{H_p}^n}{\Delta t} = -\beta_v S_{H_p}^{n+1} I_v^n - \beta_v S_H^{n+1} I_{v_p}^n - d S_{H_p}^{n+1}, \\ \frac{i_{H_p}^{k+1,n+1} - i_{H_p}^{k,n}}{\Delta t} = -\frac{\partial}{\partial p} (\alpha_{k+1} + \gamma_{k+1} + d) i_H^{k+1,n+1} - (\alpha_{k+1} + \gamma_{k+1} + d) i_{H_p}^{k+1,n+1}, \\ i_{H_p}^{0,n+1} = \beta_v S_{H_p}^{n+1} I_v^n + \beta_v S_H^{n+1} I_{v_p}^n, \\ \frac{S_{v_p}^{n+1} - S_{v_p}^n}{\Delta t} = -S_{v_p}^{n+1} \sum_{k=1}^M \beta_H^k i_H^{k,n+1} - S_v^{n+1} \sum_{k=1}^M \frac{\partial \beta_H^k}{\partial p} i_H^{k,n+1} - S_v^{n+1} \sum_{k=1}^M \beta_H^k i_{H_p}^{k,n+1} - \mu S_{v_p}^{n+1}, \\ \frac{I_{v_p}^{n+1} - I_{v_p}^n}{\Delta t} = S_{v_p}^{n+1} \sum_{k=1}^M \beta_H^k i_H^{k,n+1} + S_v^{n+1} \sum_{k=1}^M \frac{\partial \beta_H^k}{\partial p} i_H^{k,n+1} + S_v^{n+1} \sum_{k=1}^M \beta_H^k i_{H_p}^{k,n+1} - \mu I_{v_p}^{n+1}, \end{array} \right.$$

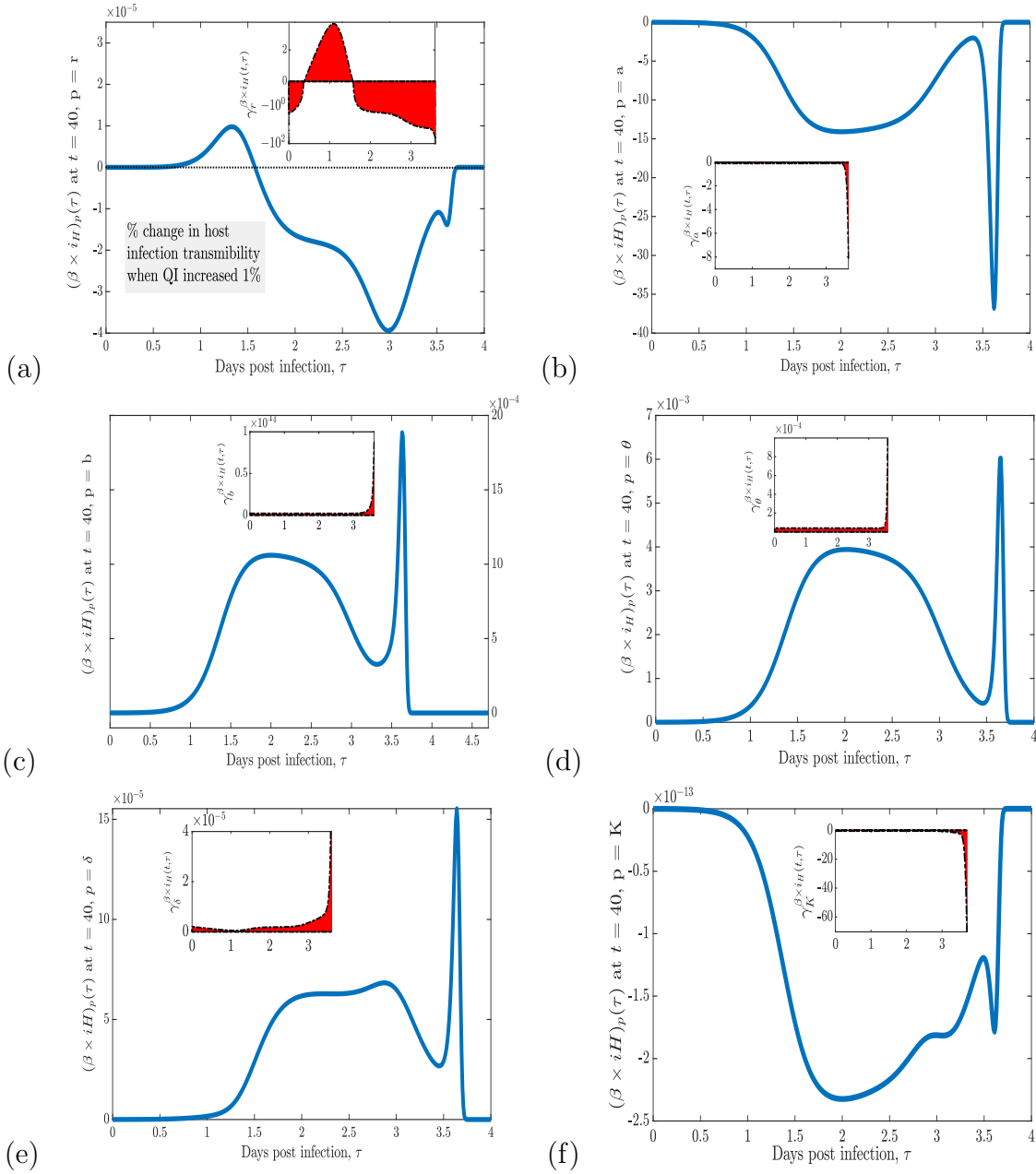


FIGURE A.8. How infection transmissibility of hosts (with different infection group τ) changes when quantity of interest (QI) such as an immune parameter p is increased by 1%. At initial phase of epidemic ($t = 40$ days after epidemic started), the percentage change in infection transmissibility among infected host groups is the largest when the change is occurred in parasite growth rate r , comparing to the rest of the immune parameters.

where the system is discretized on the domain $D = \{(\tau, t) : 0 \leq \tau \leq A, 0 \leq t \leq T\}$, the grid sizes for time (Δt) and age ($\Delta \tau$) are chosen to be the same $\Delta t = \Delta \tau$, and $T = N \Delta t$ and $A = M \Delta \tau$. We approximate the value at each grid point (τ_k, t_n) , $\tau_k = k \Delta \tau$, $t_n = n \Delta t$, $k = 1, \dots, M$, $n = 1, \dots, N$, which are denoted by $S(t_n) \approx S^n$, $i_H(\tau_k, t_n) \approx$

$i_H^{k,n}$, $\beta_H(\tau_k) \approx \beta_H^k$ along with derivatives $\frac{\partial S_H(t_n)}{\partial p} \approx S_{H_p}^n$, $\frac{\partial i_H(\tau_k, t_n)}{\partial p} \approx i_{H_p}^{k,n}$, $\frac{\partial S_v(t_n)}{\partial p} \approx S_{v_p}^n$, $\frac{\partial I_v(\tau_k, t_n)}{\partial p} \approx I_{v_p}^{k,n}$. Lastly, the linked parameters $\beta_H(\tau_k)$, $\alpha(\tau_k)$, $\gamma(\tau_k)$ and their derivatives with respect to the model parameters p are pre-calculated following the numerical method as described in Section 3.

Furthermore recall that whenever $\mathcal{R}_0 > 1$, independent from (non-zero) initial conditions, the solutions converge to the EE \mathcal{E}^* . In addition to that, in the previous section, we analytically and numerically derive the sensitivity index, $\gamma_{\mathbf{p}}^{i_H^*}$ from the explicit expression of $i_H^*(\tau)$, given in (2.5).

The subfigures (a)-(d) in Fig.A.8 display the sensitivity, $\frac{d\beta \times i_H(\tau)}{d\mathbf{p}}$ of the infection transmissibility (of infected individuals) with respect to immunological parameters $\mathbf{p} \in \{r, a, b, \theta, \delta, K\}$ (at varying host infection age τ) $t = 40$ days after epidemic starts, which we called initial phase of epidemic (see Fig.3.3(a)). The inserted subfigures in each figure display % of change in host infection transmissibility when QI increased 1% at infection age τ ; i.e. $\gamma_{\mathbf{p}}^{\beta \times i_H}(\tau)$. In the inserted subfigure of Fig.A.8(a), we observe that the changes in the immune parameters can modulate the infection transmissibility of distinct infected host groups significantly. For example, at the initial phase of the epidemic, in particular $t = 40$ days after epidemic started, 1% increase in-host parasite growth rate r leads up to 4% increase in the infectivity of individuals whom infected approximately at least 1.6 and at most 3.6 days ago. Notice that the infectious period for hosts is approximately 4 days. Significant reduction in the host infection transmissibility when host infected more than 3.6 days ago (before virus clearance) is due to increase in disease death rate induced by larger parasite growth, and instant large immune response in this infectious time interval. On the other hand, the decrease in the transmission infectivity of individuals whom got infected up to 1.6 days ago, might be due to stronger immune response leading containment of virus in-host, or causing death. At initial phase of epidemic, the percentage change in infection transmissibility among infected host groups is the largest when the change is occurred in parasite growth rate r , comparing to the rest of the immune parameters a in Fig.A.8(b), b in Fig.A.8(c), θ Fig.A.8(d), δ in Fig.A.8(e), K Fig.A.8(f).

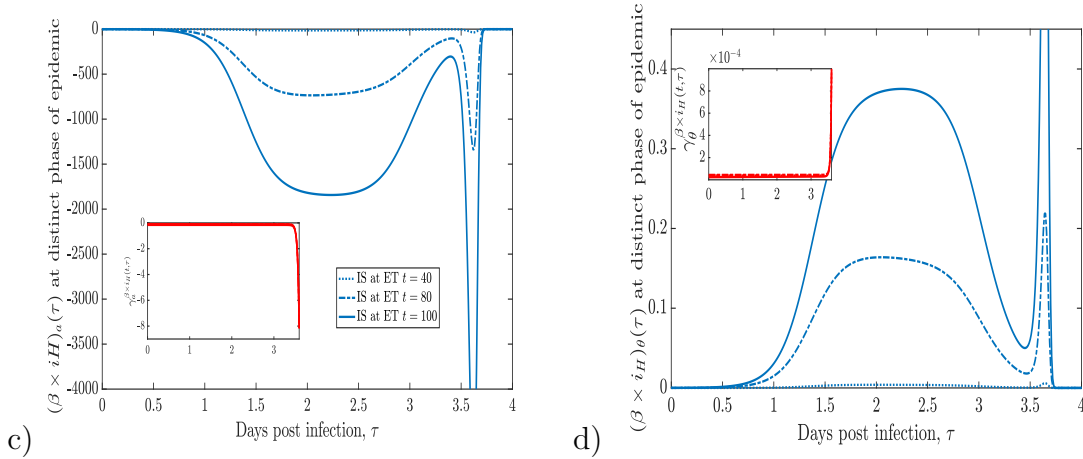


FIGURE A.9. Sensitivity of infection transmissibility at distinct epidemic time t to immune parameters a , and θ .

ACKNOWLEDGEMENT

The authors thank two anonymous reviewers for their helpful comments and feedback on the manuscript, and Mac Hyman of Tulane University for his helpful discussions. Hayriye Gulbudak was supported by NSF grant (DMS-1951759) and Simons Foundation/SFARI(638193). The research of Necibe Tuncer was partially supported by NSF grant (DMS-1951626).

REFERENCES

- [1] R. M. Anderson and R. May. Coevolution of hosts and parasites. *Parasitology*, 85(2):411–426, 1982.
- [2] O. Angulo, F. Milner, and L. Segal. A sir epidemic model structured by immunological variables. *Journal of Biological Systems*, 21(04):1340013, 2013.
- [3] C. Browne, H. Gulbudak, and G. Webb. Modeling contact tracing in outbreaks with application to ebola. *Journal of theoretical biology*, 384:33–49, 2015.
- [4] C. J. Browne, H. Gulbudak, and J. C. Macdonald. Differential impacts of contact tracing and lockdowns on outbreak size in covid-19 model applied to china. *Journal of Theoretical Biology*, 532:110919, 2022.
- [5] E. A. Fischer, G.-J. Boender, G. Nodelijk, A. A. De Koeijer, and H. J. Van Roermund. The transmission potential of rift valley fever virus among livestock in the netherlands: a modelling study. *Veterinary research*, 44(1):58, 2013.
- [6] C. for Disease Control, P. (CDC, et al. Rift valley fever outbreak—kenya, november 2006-january 2007. *MMWR. Morbidity and mortality weekly report*, pages 73–76, 2007.
- [7] C. Fraser, K. Lythgoe, G. E. Leventhal, G. Shirreff, T. D. Hollingsworth, S. Alizon, and S. Bonhoeffer. Virulence and pathogenesis of hiv-1 infection: an evolutionary perspective. *Science*, 343(6177):1243727, 2014.
- [8] H. Gaff, C. Burgess, J. Jackson, T. Niu, Y. Papelis, and D. Hartley. Mathematical model to assess the relative effectiveness of rift valley fever countermeasures. *International Journal of Artificial Life Research (IJALR)*, 2(2):1–18, 2011.
- [9] H. D. Gaff, D. M. Hartley, and N. P. Leahy. An epidemiological model of rift valley fever. *Electronic Journal of Differential Equations (EJDE)[electronic only]*, 2007:Paper–No, 2007.
- [10] A. Gandolfi, A. Pugliese, and C. Sinisgalli. Epidemic dynamics and host immune response: a nested approach. *Journal of mathematical biology*, 70(3):399–435, 2015.
- [11] M. A. Gilchrist and A. Sasaki. Modeling host–parasite coevolution: a nested approach based on mechanistic models. *Journal of Theoretical Biology*, 218(3):289–308, 2002.

- [12] H. Gulbudak. An immuno-epidemiological vector-host model with within-vector viral kinetics. *Journal of Biological Systems*, 28(02):233–275, 2020.
- [13] H. Gulbudak and C. J. Browne. Infection severity across scales in multi-strain immuno-epidemiological dengue model structured by host antibody level. *Journal of mathematical biology*, 80(6):1803–1843, 2020.
- [14] H. Gulbudak, V. L. Cannataro, N. Tuncer, and M. Martcheva. Vector-borne pathogen and host evolution in a structured immuno-epidemiological system. *Bulletin of mathematical biology*, 79(2):325–355, 2017.
- [15] A. Handel and P. Rohani. Crossing the scale from within-host infection dynamics to between-host transmission fitness: a discussion of current assumptions and knowledge. *Philosophical Transactions of the Royal Society of London B*, 370(1675):20140302, 2015.
- [16] T. Honjo, K. Kinoshita, and M. Muramatsu. Molecular mechanism of class switch recombination: linkage with somatic hypermutation. *Annual review of immunology*, 20(1):165–196, 2002.
- [17] J. Macdonald, C. Browne, and H. Gulbudak. Modelling covid-19 outbreaks in usa with distinct testing, lockdown speed and fatigue rates. *Royal Society Open Science*, 8(8):210227.
- [18] P. Magal and C. McCluskey. Two-group infection age model including an application to nosocomial infection. *SIAM Journal on Applied Mathematics*, 73(2):1058–1095, 2013.
- [19] J. Morrill, F. Knauert, T. Ksiazek, J. Meegan, and C. Peters. Rift valley fever infection of rhesus monkeys: implications for rapid diagnosis of human disease. *Research in virology*, 140:139–146, 1989.
- [20] S. C. Mpeshe, H. Haario, and J. M. Tchuente. A mathematical model of rift valley fever with human host. *Acta biotheoretica*, 59(3-4):231–250, 2011.
- [21] P. Munyua, R. M. Murithi, S. Wainwright, J. Githinji, A. Hightower, D. Mutonga, J. Macharia, P. M. Ithondeka, J. Musaa, R. F. Breiman, et al. Rift valley fever outbreak in livestock in kenya, 2006–2007. *The American journal of tropical medicine and hygiene*, 83(2_Suppl):58–64, 2010.
- [22] M. Pepin, M. Bouloy, B. H. Bird, A. Kemp, and J. Paweska. Rift valley fever virus (bunyaviridae: Phlebovirus): an update on pathogenesis, molecular epidemiology, vectors, diagnostics and prevention. *Veterinary research*, 41(6):61, 2010.
- [23] N. Tuncer, H. Gulbudak, V. L. Cannataro, and M. Martcheva. Structural and practical identifiability issues of immuno-epidemiological vector–host models with application to rift valley fever. *Bulletin of mathematical biology*, 78(9):1796–1827, 2016.
- [24] Y. Xiao, J. C. Beier, R. S. Cantrell, C. Cosner, D. L. DeAngelis, and S. Ruan. Modelling the effects of seasonality and socioeconomic impact on the transmission of rift valley fever virus. *PLoS neglected tropical diseases*, 9(1), 2015.

DEPARTMENT OF MATHEMATICS, UNIVERSITY OF LOUISIANA AT LAFAYETTE 217 MAXIM DOUCET HALL, P.O. BOX 43568, LAFAYETTE, LA
Email address: hayriye.gulbudak@louisiana.edu

DEPARTMENT OF MATHEMATICS, UNIVERSITY OF TEXAS AT SAN ANTONIO, ONE UTSA CIRCLE, SAN ANTONIO, TX 78249
Email address: zhuolin.qu@utsa.edu

SCHOOL OF MATHEMATICAL AND STATISTICAL SCIENCES, ARIZONA STATE UNIVERSITY, 825 WEXLER HALL, PO BOX 871804, TEMPE, AZ 85287
Email address: fmilner@asu.edu

DEPARTMENT OF MATHEMATICAL SCIENCES, FLORIDA ATLANTIC UNIVERSITY, SCIENCE BUILDING, ROOM 234 777 GLADES ROAD BOCA RATON, FL 33431
Email address: ntuncer@fau.edu